



Case Report

Perioperative Benefits of a 3D Printed Spine Biomodel in the Setting of Congenital Scoliosis Surgery

Dean C. Perfetti¹, Stanley Kisinde¹, Theodore A. Belanger² and Isador H. Lieberman^{1,*}

¹ Scoliosis & Spine Tumor Center, TBI, Plano, TX 75093, USA

² Texas Back Institute, TBI, Rockwall, TX 75032, USA

* Correspondence: ilieberman@texasback.com

Abstract: The spine community is continuously adding to its armamentarium of intraoperative techniques for visualization and instrumentation of the spine. Recently, three-dimensional printed spine models were introduced for use in preoperative planning, surgical simulation, and intraoperative guidance. We present a 14-year old African male with congenital kyphoscoliosis, small stature, an obvious gibbus deformity and coronal imbalance, who underwent a three-staged posterior surgical correction procedure, during which a 3D-printed spine biomodel was utilized for better appreciation of his complex spinal deformity patho-anatomy. During the first stage of the procedure, he developed diminished lower extremity motor strength bilaterally and bowel/bladder control, but, following his third stage procedure and with focused rehabilitation efforts, he has regained full control of his bowel and bladder function, and is able to ambulate and perform activities of daily living independently, albeit still requiring intermittent walking support with a single forearm crutch due to residual left leg weakness. The 3D spine biomodel functioned successfully as a valuable tool and surrogate anatomic blueprint for the surgeons, enabling adequate appreciation of the complex bony anatomy which could not be easily resolved on the conventionally available imaging modalities, intraoperative navigation or robotic platform. Theoretically, up to \$2900 USD in savings, translated from the mean estimated time saved per procedure with the use 3D-printed spine models has been proposed in some studies. Therefore, 3D-printed spine models have utility in complex spinal deformity correction surgery.



Citation: Perfetti, D.C.; Kisinde, S.; Belanger, T.A.; Lieberman, I.H. Perioperative Benefits of a 3D Printed Spine Biomodel in the Setting of Congenital Scoliosis Surgery. *Surg. Tech. Dev.* **2024**, *13*, 278–293. <https://doi.org/10.3390/std13030021>

Academic Editor: Ralph Mobbs

Received: 14 March 2024

Revised: 31 July 2024

Accepted: 7 August 2024

Published: 9 August 2024



Copyright: © 2024 by the authors. Licensee MDPI, Basel, Switzerland. This article is an open access article distributed under the terms and conditions of the Creative Commons Attribution (CC BY) license (<https://creativecommons.org/licenses/by/4.0/>).

Keywords: congenital deformity; scoliosis; kyphosis; 3D-printed spine model; deformity correction

1. Introduction

Scoliosis is a structural three-dimensional spinal deformity that involves vertebral deformities in all 3 major planes: sagittal, horizontal and coronal planes [1–3]. Patients may present with pain, cardiorespiratory dysfunction and social and psychological distress due to cosmetic deformity [3,4]. In cases with severe congenital deformity, symptoms that are unamenable to non-operative treatment modalities, and those at a high risk of progressive deterioration, surgical intervention that aims to stabilize the curve and to reduce the impact on internal thoraco-abdominal organs and the neural tissues of the spine may be necessary [3,5]. Surgery involves initial osteotomies with decompressions—as required—to mobilize the spine and allow for optimal deformity correction, followed by stabilization with instrumentation fixation and fusion. The most commonly used mode of fixation today is pedicle screw instrumentation which provides a three-column fixation of the spine [3].

While often life-changing, spine surgical procedures carry an inherent risk of complications, including, but not limited to, bleeding, infection, neurological injury, injury to major vascular structures and internal organs, and misplacement of the instrumentation [6,7]. The incidence of these complications is increased in cases with severe congenital deformities of the spine due to the wide variation in the patho-anatomy of the deformed spinal structures [3].

The landscape of modern surgical safety has shifted to a proactive model that employs preventative strategies to identify and alleviate risks and complications by leveraging technological advancements, data analytics and interdisciplinary collaboration [7,8]. These have been employed pre-operatively in patient education, higher quality computed tomography (CT) and magnetic resonance (MR) imaging with 3D reconstruction that offer more intricate data to better visualize anatomic structures, and in the development of a pre-operative surgical plan. Intraoperatively, navigation and robotic-assistance have provided physicians with improved dexterity and 3D visualization allowing for greater accuracy during complex spine surgical procedures [7,9,10].

As technology advances further, the spine community continues to add to its armamentarium of pre-operative and intraoperative techniques for visualization and instrumentation of the spine. Three-dimensional (3D) printed models have been recently introduced for use in preoperative planning, surgical simulation, and intraoperative guidance for spine surgery [11–15]. These models are specifically beneficial when faced with complex spine pathology and morphology, especially during deformity, tumor, infection and severe trauma situations, where the anatomy may overwhelm intraoperative navigation or robotic assistance, even with experienced surgeons who are comfortable with freehand placement of implants [16].

3D printing has been applied to preoperative surgical planning for complex deformity spinal surgery [2,11–13,15]. This form of biomodelling reproduces the native structure's morphology from CT and/or MR image data using image processing software and a rapid prototyping apparatus [2,12]. Two dimensional planar radiographic images can give a holistic view of the anatomy, but are often difficult to interpret for complex pathology. CT and MR images enhance visualization of the disease process in three dimensions; however, they too can be difficult to decipher in complex anatomical situations.

This case demonstrates the preoperative and intraoperative benefits of a 3D-printed spine biomodel compared to standard image visualization, navigation, or robotic techniques in a complex congenital scoliosis case.

2. Materials and Methods

This is a retrospective single case review report. The patient-specific 3D-printed spine model described in this report is a solid structural print representing only the osseous components of the specific patient's entire spine and corresponding foramina. The model design was created using the Axial3D Insight Cloud-based platform (Axial Medical Printing Limited, Belfast, Northern Ireland, UK), and the model was developed from PA12 Nylon-Grey material (Proto3000, Atlanta, GA, USA) using an HP Jet Fusion 540 3D Printer (HP Inc., Palo Alto, CA, USA). 0.6 mm CT slice DICOM images data was securely uploaded to the Axial3D Insight™ platform. The platform's AI-assisted automated segmentation powered by machine learning algorithms processed the DICOM data to generate a virtual 3D model design. A quality control verification process was conducted on the 3D model design before exporting it as a stereolithography (STL) file. This STL file was then loaded onto the HP build manager to generate a 3D Print File, which was then uploaded onto the HP Jet Fusion 3D Printer as the blueprint for the printer to read. The final model was then created by Multi-jet Fusion type of 3D Printing. The process from the submission of the CT images to the delivery of the pre-operative 3D-printed spine model required 7 days. The same clinical CT images were utilized for the preparation of the 3D model as the preoperative plan for computer-assisted robotic guidance. At the time of surgery, the model was carefully placed entirely in a clear sterile bag and sealed to provide anatomic reference on the operating field.

3. Clinical Presentation

3.1. Case Description

A 14-year-old African male with congenital scoliosis, managed non-operatively since initial diagnosis at age 3 years, complained of pain while walking or lying down but no

radicular complaints or bowel or bladder issues. He had previously been hospitalized due to radiating pain in his spine at about 6 years old, but has had no additional hospitalizations since then. He was small in stature with an obvious deformity and coronal imbalance (Figures 1 and 2). Neurologic exam revealed full motor strength with no sensory deficits or myelopathic signs.



Figure 1. Initial physical examination photographs showing an individual with small stature, a congenital Gibbus deformity and coronally imbalanced.



Figure 2. Full length AP and lateral EOS images taken pre-operatively.

3.2. Diagnostic Assessment

Full-length standing scoliosis films demonstrated a congenital deformity at T12-L1; he was coronally shifted to the right and had a 100-degree thoracolumbar junctional kyphotic deformity. The severe congenital deformity was better characterized on CT images with hemivertebrae and incomplete formation of the posterior elements from T10 down through

L2, most pronounced at the T12 vertebral level. The CT images were used for pre-operative planning for the computer-navigated robotic-assisted placement of pedicle screws from T5 down to L4 across his congenital anomalies (Figures 2–5).

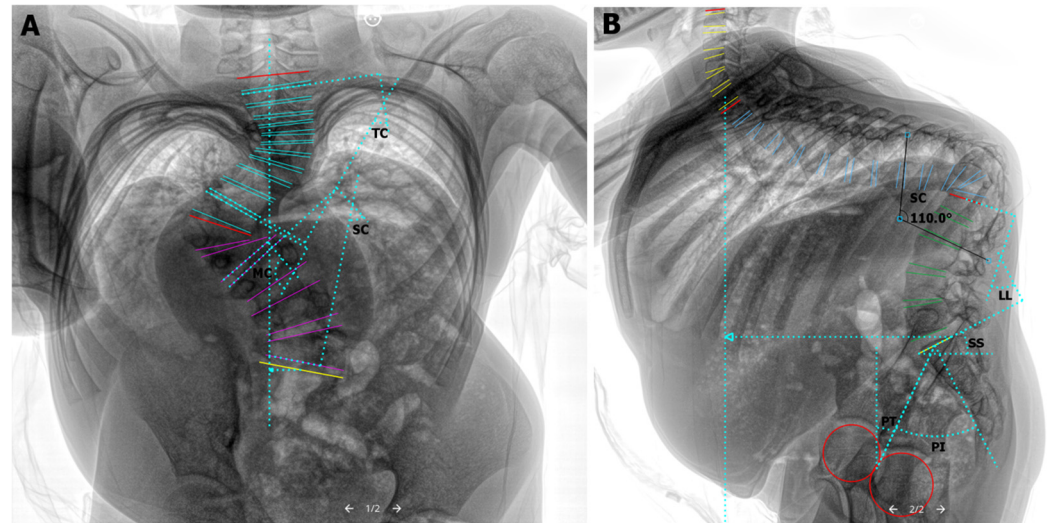


Figure 3. Standing, pre-operative total spine AP & lateral X-ray images with sagittal and coronal alignment measurements. Curve type 5C + (L)–Lenke classification of AIS [17]. (A) (Anterior-posterior)–C7PL 1.54 cm; Major Cobb [MC] 69.9°, T12 Superior-L2 Inferior; Secondary Cobb [SC] 53.8°, L3 Superior-L5 Inferior; Tertiary Cobb [TC] 38.1°, T2 Superior-T11 Inferior. (B) (Lateral)–Sagittal Pelvic Tilt [PT] 25.3°; Pelvic Incidence [PI] 52.3°; Sacral Slope [SS] 27.1°; Lumbar Lordosis [LL] 45.4°; Sagittal Cobb [SC]-thoracolumbar kyphotic deformity of 110°, T9 Superior-L2 Inferior; Thoracic Kyphosis T4-T12 69.1°.

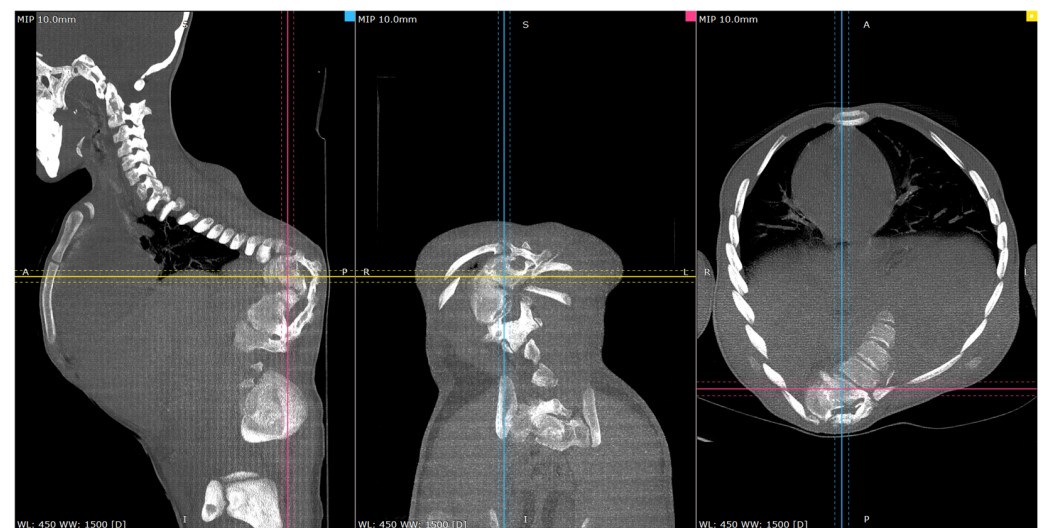


Figure 4. Representative pre-op CT scan views of the congenital deformity. Cross-reference grid lines mark the intersection of the corresponding image planes: Blue—sagittal; Pink—Coronal; Yellow—Axial views.

A 3D-printed model of the patient’s complete spine from C1 to the sacrum was obtained to facilitate preoperative surgical planning; osteotomies were also planned preoperatively on the model (Figure 6).

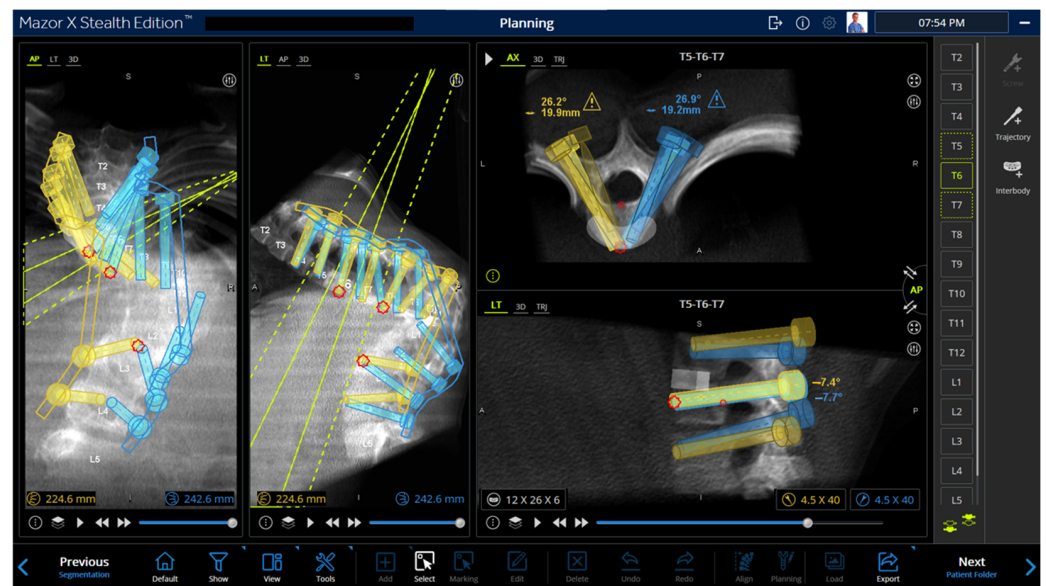


Figure 5. Pre-operative plan for computer-assisted robotic guided screw placement. Solid yellow (Left) and blue (Right) screw-shaped models are computer assisted designs of the planned screw trajectories with rods (continuous rectangular sketches) attached to them. Red rhomboid outlines indicate abutting of the planned trajectories. The area between the dotted yellow lines corresponds to that represented in the axial (AX) and lateral (LT) view windows.

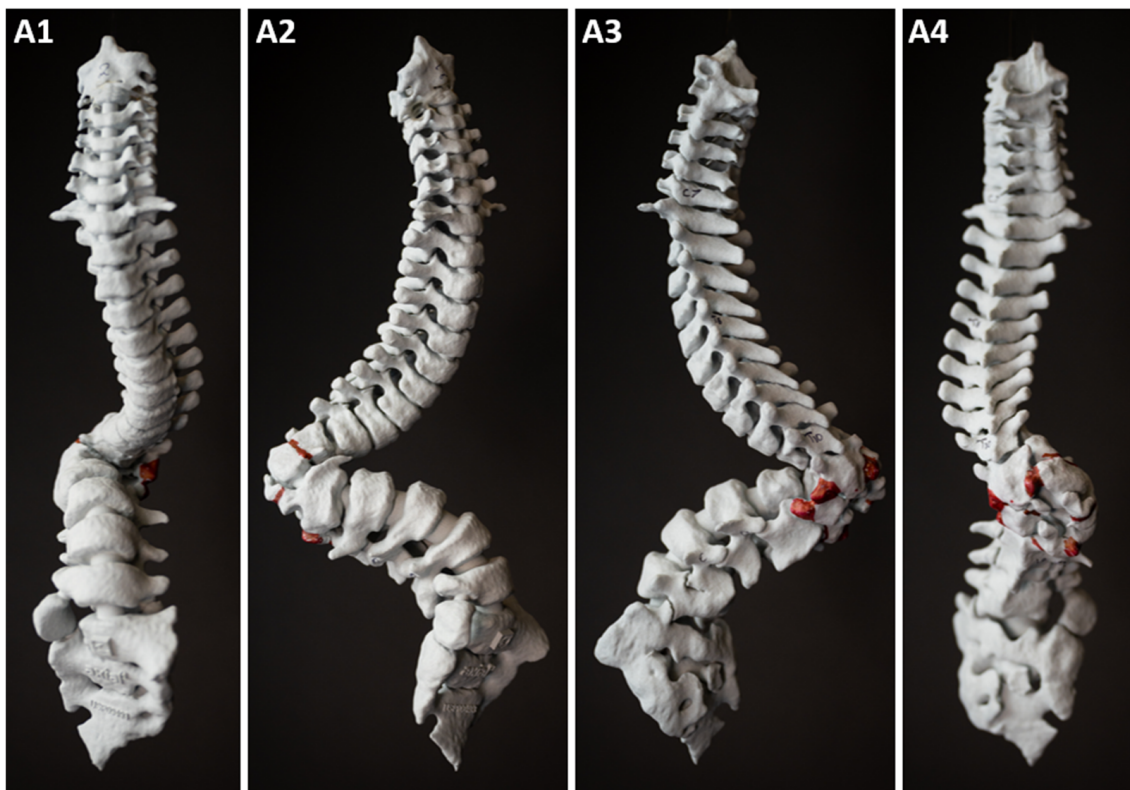


Figure 6. Cont.

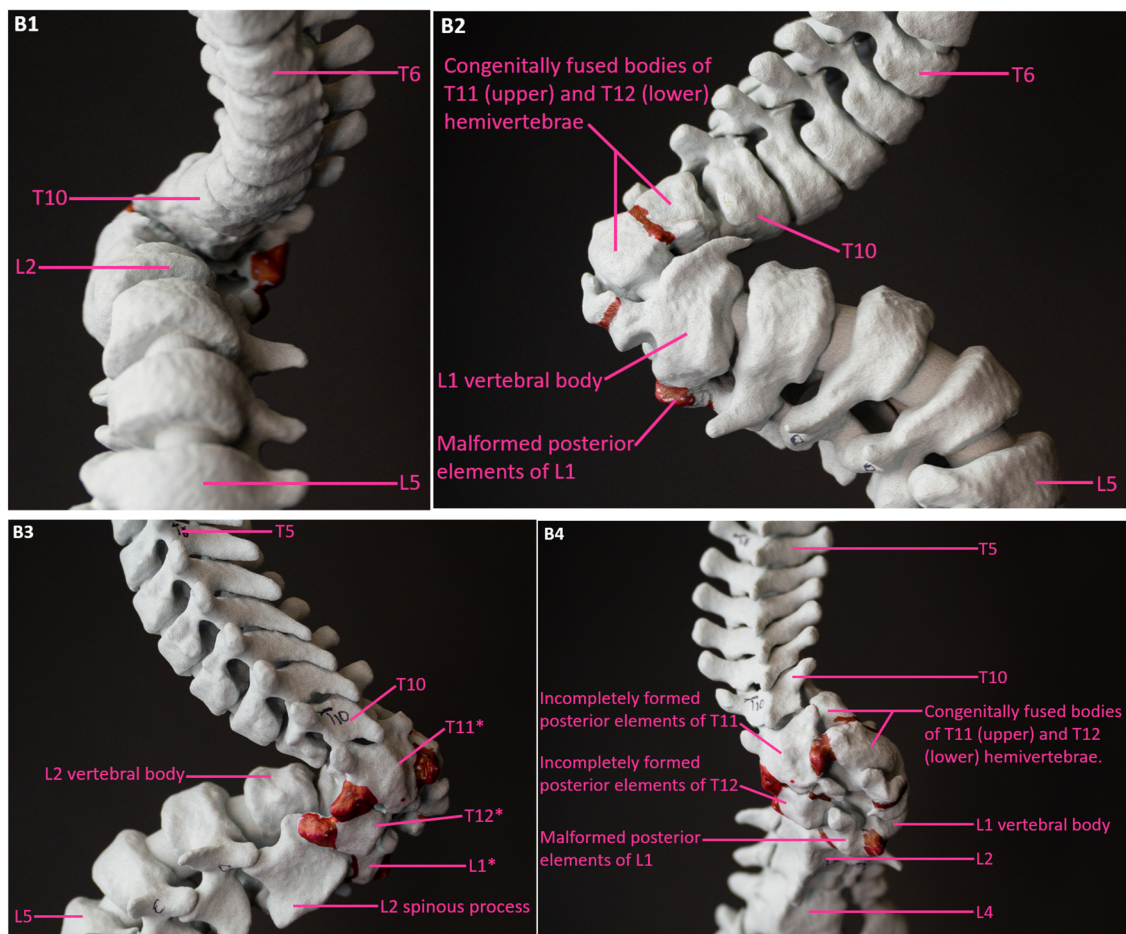


Figure 6. Full length (A) & partial (thoracolumbar) (B) images of the 3D-printed spine biomodel with resection and osteotomy boundaries marked in red. 1–Anterior, 2–Right lateral, 3–Left lateral, and 4–Posterior views. * Incompletely formed/Congenitally malformed posterior elements. T—Thoracic; L—Lumbar.

3.3. Therapeutic Intervention-Surgery

The original plan was a 2-stage, all-posterior procedure, the initial stage involving osteotomies and pedicle screw instrumentation without rod placement, followed by traction, while the second stage would involve vertebral column resection of the congenital zone and final instrumentation, deformity correction and fusion. Spinal cord monitoring with somatosensory evoked potentials (SSEPs), motor evoked potentials (MEPs) and electromyography (EMG) monitoring were utilized, and the 3D spine model was placed in a clear, sterile, sealed bag for visualization during the surgery.

Stage 1 of the procedure involved partial thoracoplasties of T10–T12 ribs to gain access, and then partial corpectomies of vestigial vertebral bodies T11, T12 and L1 and resection of the vestigial discs at T11–T12 and T12–L1 in an extra cavitory fashion, along with Schwab type 2 facet osteotomies at T5–T11 and L2–L4. The resected bone was morselized and saved for the second stage in an intramuscular pouch. The robotic platform was utilized for initial instrumentation, but by virtue of the deformity, registration of the AP and oblique fluoroscopic images to the CT scan images was difficult, enabling only left sided L3 and L4 pedicle screw placement. A sublaminar wire was then placed manually at T8 to act as a marker for registration during the second stage. During surgery, the model was used to confirm the boundaries of dissection, provide more accurate orientation, localize the multiple congenital anomalies and dysplastic landmarks, and as a reference for the pre-planned osteotomies (Figure 6).

During wound closure, the SSEPs started diminishing. The patient was placed supine and monitored for 45 min. As the potentials remained unpredictable, reinforced by diminished lower extremity motor strength bilaterally on the wake-up test—ASIA C, he was repositioned back prone on the operating table, the back was re-prepped and draped, and the surgical site was re-opened. At re-opening, no large hematoma or other fluid collection was noted. A more substantial complete laminectomy across the entire congenital segment from T10 through L2 was performed. The cord remained draped over the congenital segment. There was no obvious gross instability of the spine. SSEPs did not return to baseline and only a weak right sided quadriceps motor evoked potential (MEP) was present. The wound was reclosed. Despite the original plan, halo traction for gradual lengthening of the spine was not applied to avoid any further inadvertent injury to the cord.

After close overnight monitoring in the ICU, and noting positional response to motor function, the patient was returned to the OR for temporary spinal stabilization through the previous midline incision from T5 to L4. Using intraoperative CT imaging, with the T8 sublaminar wire as a fiducial marker, accurate registration was achieved for the placement of pedicle screws under robotic guidance from T5–T9 with solid purchase. The robotic platform was not able to accurately register screws from T10–L2, so the 3D model was used to guide manual implantation of right-sided L2–L4 screws.

Three rods were then cut, contoured to the desired shapes in the sagittal and coronal planes, and fastened to the screws. On the left side, side-to-side connectors were used to connect two rods in the thoracic and lumbar spine, while on the right side, a transition rod was contoured and it spanned the entire congenital segment. Strategic distraction, compression and de-rotation were used to achieve correction (Figure 7). Throughout the procedure, spinal cord monitoring revealed strong MEPs to the quadriceps but no recovery of MEPs below the knees.

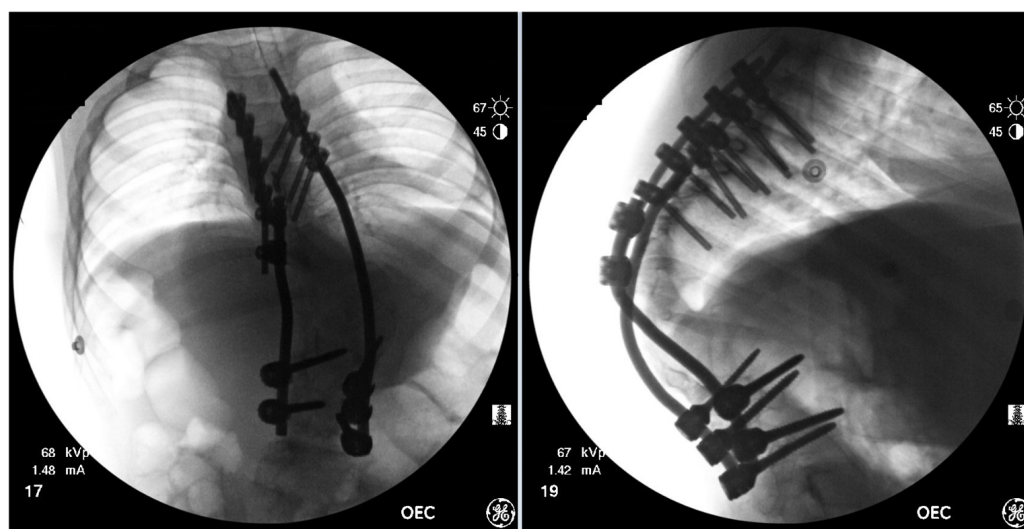


Figure 7. AP & Lateral fluoroscopy images of temporary spinal instrumentation stabilization.

In the immediate post-operative period, new-onset difficulties with continence and with continued bilateral lower extremity (BLE) weakness prompted a third visit to the OR for completion of T11–12 corpectomies and resection of the associated vestigial disc spaces through the posterior incision. Using the 3D model on the surgical field as guidance, two additional points of fixation were placed manually in the body of T10 and the remnant of L1 on the right side, and a fibular strut graft was placed anteriorly between the two vertebral bodies (Figure 8).



Figure 8. AP & Lateral fluoroscopy images of the final instrumentation & deformity correction.

Strategic distraction, compression and de-rotation were used to achieve further correction—reduction of the kyphosis—slowly, using the rod exchange maneuver multiple times with temporary rods. Once substantial correction was achieved, these were exchanged with definitive rods placed from T5 to L4. After fine-tuning the correction, the MEPs did improve with tibialis anterior MEPs returning on both sides. Two cross links were placed over the vertebral body resection site. With the final correction achieved, further bone graft was applied across the posterolateral gutters, the facet joints and the corpectomy defect site, and the wound was closed (Figure 8).

During surgery, the model was placed in a clear, sterile, sealed plastic bag for visualization. It was used to confirm the boundaries of dissection, provide more accurate orientation, localize the multiple congenital anomalies and dysplastic landmarks, and as a reference for the pre-planned osteotomies (Figure 6) and trajectories for the manually-implanted screws.

3.4. Follow-Up and Outcome

His multi-stage surgery resulted in loss of BLE motor function, bowel and bladder incontinence, and a long postoperative recovery and rehabilitation. With focused rehabilitation efforts, over 4 months, he steadily recovered and was able to walk independently, only requiring a walker intermittently. Likewise, bowel function had improved with a bowel training regimen, while he reported being able to sense urinary urgency and having accidents only rarely at night.

Postoperative CT scan images verified bone formation across the congenital defect, and clinically, he was balanced in both sagittal and coronal planes (Figures 9–12).

At the time of submitting this manuscript, about 16 months post-operatively, the patient is recovered substantially and thriving well with no new complaints reported. The patient is able to ambulate and perform activities of daily living independently, albeit still requiring walking support only intermittently with a forearm crutch due to residual left leg intermittent weakness. He has regained full control of his bowel and bladder but he still has issues with recurrent urinary tract infections.



Figure 9. Full-length AP and lateral EOS images—4-months Post-operatively.



Figure 10. Representative post-op CT scan views—4-months Post-operatively. Cross-reference grid lines mark the intersection of the corresponding image planes: Blue—sagittal; Pink—Coronal; Yellow—Axial view.

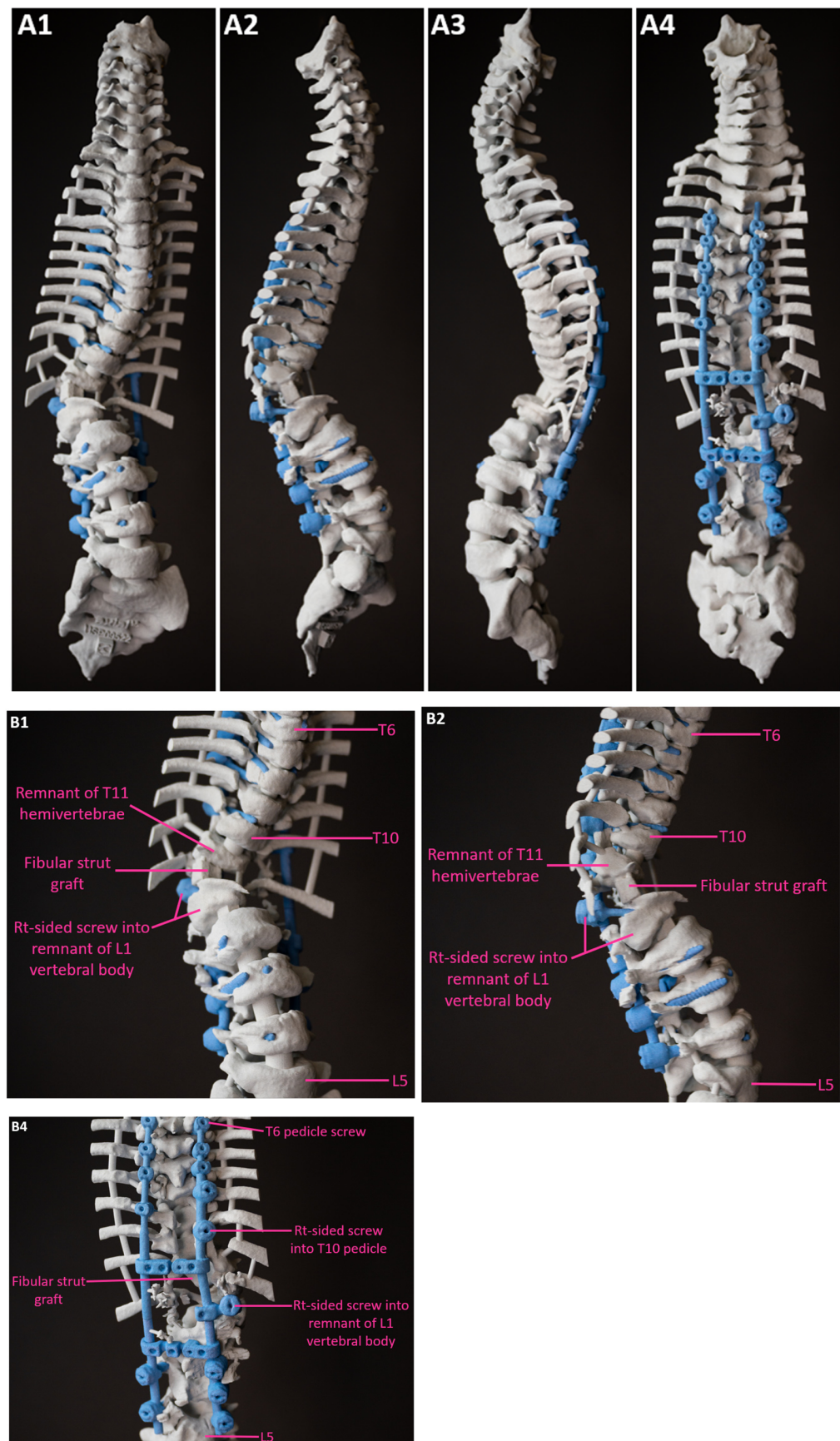


Figure 11. Full length (A) & partial (thoracolumbar) (B) images of the post-operative 3D spine biomodel. 1—Anterior, 2—Right lateral, 3—Left lateral, and 4—Posterior views. T—Thoracic; L—Lumbar.



Figure 12. Pre vs. Post-operative clinical examination photographs showing correction of the severe thoracolumbar junctional kyphotic deformity and coronal balance with the patient's head positioned neutrally above the rest of the body postoperatively.

4. Discussion

4.1. 3D-Printed Spine Model vs. Robotics and Navigation

Successful treatment of complex spinal pathologies such as congenital scoliosis demands exacting preoperative planning and meticulous surgical technique. Although robotics and navigation have allowed for more accuracy and are growing in application, these modalities are limited during critical moments involving instrumentation and bone work around a severe congenitally deformed spinal segment [2,9]. 3D biomodels are instrumental during these technological lapses where free-hand techniques need to be utilized. Aided by the model during this case, we were able to more easily identify the deformity, and successfully performed the planned osteotomies and vertebrectomies, while protecting vital neurovascular structures.

4.2. Consent and Education

The model was utilized in all aspects of perioperative management from patient education and consent, to clinical discussions, intraoperative dissection and decision making. It also aided in trainee surgeon education and clearer communication between the operating surgeons and the OR team. Multiple studies have similarly reported the adoption of 3D printed biomodels for surgical training while avoiding the ethical, economic and anatomic variation barriers that are associated with the use of cadavers [14,16,18].

4.3. 3D Spine Model vs. Conventional Imaging Modalities for Surgical Planning

The model helped us to predict the complexity of the surgical procedure beforehand by giving us a better appreciation of the challenging spinal deformity patho-anatomy than the conventional imaging modalities. This model was also accurate in its structural representation of the deformity, and free of artifacts or thermal surface deformation given the fact that during surgery, it was wrapped in a clear sterile bag, thereby avoiding the effects of pressurized autoclave heat on its integral structure. 3D models have been shown to better aid in the development of a presurgical plan, reduce the probability of encountering unexpected anatomy or relative positioning of anatomic structures, allow for evaluation of different alternatives for surgical approach, and pre-operative ordering of the required

instrumentation and device sets for multi-stage spine surgical procedures [14,19]. Of note, the use of the model did not affect the choice of implants utilized during the procedure.

4.4. Intraoperative Anatomic Reference

Despite the extensive experience of the surgical team, the authors found that anatomical reference provided by the 3D biomodel contributed an additional sense of security when exposing vestigial segments, performing the osteotomies and vertebral column resection, and when instrumenting around the deformity. The model was used by positioning it parallel to the patient's open incision, "looking around the corner" by rotating it, and simulating screw trajectories on the surgical field. In a previous case report of an anterior L5-S1 osteophyte causing L5 radiculopathy due to L5 n. root entrapment, CT scan data was extrapolated to create a 3D model. Similar to our case, the surgeons repeatedly referred to the model intraoperatively to better understand and visualize the rare patho-anatomy closely represented by the model, and were able to successfully resect the osteophyte and safely decompress the L5 n. root via an anterior retroperitoneal approach [20].

4.5. Other Intraoperative Parameters

3D printing technology has been shown to result in decreased surgical time, less bleeding, decreased decision-making time and reduced number of intraoperative fluoroscopy cycles [14,19]. Izatt et al. also found that the biomodels reduced operating time by 22%, which they attributed to higher surgical confidence during dissection, and fewer intra-operative complications [12]. Due to the high degree of complexity of the congenital deformity and the development of neurological complications in our case, the patient underwent a 3-stage surgical procedure. Additionally, the patient's history of congenital scoliosis correlates with a high probability of having other underlying problems with other mesodermal derived tissues, and his postoperative course subsequently did unmask a hydronephrosis that was not appreciated preoperatively, even with medical clearance. Therefore, while his bowel incontinence improved, his bladder incontinence continued due to this tandem hit on the urogenital and neurologic systems, specifically from the spinal cord injury during deformity correction at the thoracolumbar junction. Even with this less than optimal outcome, the 3D-printed model played a significant role, without which the achieved deformity correction and other positive surgical parameters would not have been realized.

4.6. Financial Implications of Using 3D Printed Spine Biomodels on the Hospital

Even as utility and cost data regarding the launch and maintenance of 3D printing in a hospital can help to inform health care budgets, there is a paucity of such information. In one of a few landmark papers on clinical practice management, Ravi et al. studied the utility and costs following the launch of a 3D printing clinical service in its first year of inception in an academic hospital setting. In their experience, the total startup cost which included professional costs, cost of purchasing 3D printers and their warranties, all materials and supplies, and a workstation with dedicated 3D printing software was \$213,450 USD. This translated into a total cost of \$2737 USD per model for 78 models produced [21]. 3D printed biomodels have been shown to potentially offer advantages such as greater accuracy in diagnosis of pathology, better pre-operative planning of the surgical workflow including better communication within the surgical team, ordered preparation of the necessary instrumentation for multi-step and revision procedures, decreased surgical and/or procedural time, decreasing the probability of the surgical team encountering unexpected anatomy or relative positioning of structures and/or devices, less intraoperative blood loss, decreased intraoperative fluoroscopy time and higher accuracy rates of screw/hardware placement [22]. Benchmarking on the clinical benefit of reduced operation time with the use of 3D biomodels as a function of a more evolved understanding of the pathologic anatomy, surgical approach and pre-operatively planned instrumentation decisions, Ravi et al. reported that the mean estimated procedure time saved was 29.9 min. Given the estimated

cost of \$36–\$97 USD per minute for procedure rooms, a theoretical translation would yield \$1076–\$2900 in savings per procedure with the use of 3D biomodels [14,21,23,24]. We are unable to provide a cost value for the 3D spine model in our case as it was donated. While this model was indicated for severe congenital deformity of the spine, the models in the Ravi study were indicated for preoperative planning and management of cardiac, major vascular, orthopedic and maxillofacial surgeries, and head & neck and renal tumors [21]. Also, because of singularity and complications that were encountered during the procedure in our report, we are unable to extrapolate any information related to the duration of surgery or any theoretical savings therein.

Additionally, the cost of 3D printing in their hospital was greatly comparable to the estimated cost of outsourcing 3D printing to industry, that is, \$2737 vs. \$2467 per model respectively [21]. This further supports the hybrid option utilized in our case to outsource the 3D model from an already existent 3D printing establishment.

4.7. Limitations

The major obstacles to using 3D biomodels are the high cost of production—large 3D-printers, printing materials, 3D-reconstruction software, large-scale setup and human resource—lengthy production time and varying physical characteristics of the printing materials [2].

The 3D printing industry continues to grapple with significant background costs. Establishing a sizable 3D printing factory entails considerable upfront investment, particularly in procuring large-scale equipment. Organizations must also allocate resources for ongoing research and development in order to keep pace with the rapidly evolving technological landscape [25]. Historically, hospitals have leveraged their affiliations with universities and engineering programs to offset some of these costs [26]. Today, more hospitals are adopting a hybrid approach to tackle these constraints, such as was the case in our report, working with already existent large-scale 3D printing establishments like Axial3D (Axial Medical Printing Limited, Belfast, Northern Ireland, UK) that offers a cloud-based service for the secure transfer of data and image segmentation without the need for integration into the hospital's infrastructure [27].

The use of AI-assisted automated segmentation powered by machine learning algorithms allows for a patient-specific 3D model to be segmented quicker than with traditional manual segmentation. Using the traditional method, an engineer or radiologist will select a threshold value within the Hounsfield unit range for bone and then utilize a segmentation editor to manually segment anatomical structures slice by slice. This latter method is highly time-intensive, requiring meticulous separation of anatomy pixel by pixel. AI-assisted segmentation was used in the production of the model utilized in our case and this reduced additional manual segmentation time by approximately 12 h. This resulted in us receiving the model fairly faster—within 7 days of placing the order for the model and delivering the DICOM image data via the Axial3D Insight cloud-based platform. The other important processes that accounted for this duration include: initial back and forth communications between the surgeon and the engineering team to confirm vital anatomic structures to be included in the model, verification and validation of the 3D design, 3D printing and then shipping the physical model. Because of the intricate anatomy, complexity of the congenital deformity and the size of the spine for our case, the 3D printing process alone lasted about 72 h.

The process of segmentation is also greatly affected by the quality and type of the images. The presence of factors such as metal artifact noise and low-resolution quality of scan image data can significantly prolong the process of manual segmentation. Once again, the use of AI-assisted automated segmentation powered by machine learning algorithms can help overcome this problem as the algorithms can be trained on image data sets with metal artifacts and bone to pick up the distinction between the two, thereby further reducing the duration of the segmentation process. This is also very important as accuracy

of the segmentation process is crucial to the anatomic accuracy of the 3D-printed model to that of the specific patient's spine [3].

Therefore, this modality is presently not yet suitable for urgent or emergent spine surgical cases, although, with further emergence of progressive technologies in machine learning and artificial intelligence, the production process will continue to shorten, and the technology will become more accessible and less costly [16].

Due to the inherent physical characteristics of the printing materials, 3D-printed models are rigid and opaque leading to inability to accurately reproduce natural tissue compliance and to visualize inside the solid model, respectively [2,19]. We were, however, able to visualize the 'inside'—the central canal—of the model through its numerous foramina.

Our report also features only a single case, so, we are unable to provide any quantitative, comparative information regarding the effect of the use of the 3D biomodel on different surgical parameters and outcomes, as well as on its use in comparison to conventional imaging modalities beyond the scope of this individual case.

5. Conclusions

3D-printed spine models have utility in complex spinal deformity correction procedures. Theoretical financial benefits extrapolated from temporal savings per procedure involving their use have been proposed in some studies. However, the additional time needed for, and the high cost of, production of such models may limit their adaptation into some settings.

Future Research Directions

We plan to continue collecting data on subsequent patients during whose spinal surgical procedures a 3D-printed model will be utilized. Additionally, prospective studies assessing the surgical and patient reported outcomes following the use, or not, of 3D printed spine anatomic models during complex spinal deformity correction surgeries would help provide more information and enhance the acceptance of 3D-printed models in spine surgery.

Author Contributions: All the authors whose names appear on the submission made substantial contributions to the conception and design of the work. D.C.P. and S.K. drafted the work and D.C.P., S.K., T.A.B. and I.H.L. revised it critically for important intellectual content. D.C.P., T.A.B. and I.H.L. were part of the team that performed the surgery and have been following up the patient. D.C.P., S.K., T.A.B. and I.H.L. approved the version to be published and agree to be accountable for all aspects of the work in ensuring that questions related to the accuracy or integrity of any part of the work are appropriately investigated and resolved. All authors have read and agreed to the published version of the manuscript.

Funding: This research received no external funding.

Institutional Review Board Statement: The study was conducted in accordance with the Declaration of Helsinki, and received ethical exemption from IRB oversight, via the IRB-C.A.R.R.I.E. system, submission ID#2023-909, by the Institutional Review Board of Medical City Plano.

Informed Consent Statement: Written informed consent for the procedure and for publication of this report was obtained from the patient and guardian.

Data Availability Statement: No new data were created or analyzed in this study. Data sharing is Not Applicable to this article.

Acknowledgments: We thank Phillip Slaughter (TBI) for taking the photos of the 3D spine biomodels. We also acknowledge receipt of technical information about the 3D printing process from the AXIAL3D team represented by Sophie McIlveen; s.mcilveen@axial3d.com.

Conflicts of Interest: The authors declare no conflicts of interest.

References

1. Illés, T.; Tunyogi-Csapó, M.; Somoskeöy, S. Breakthrough in three-dimensional scoliosis diagnosis: Significance of horizontal plane view and vertebra vectors. *Eur. Spine J.* **2011**, *20*, 135–143. [[CrossRef](#)] [[PubMed](#)]
2. Martelli, N.; Serrano, C.; van den Brink, H.; Pineau, J.; Prognon, P.; Borget, I.; El Batti, S. Advantages and disadvantages of 3-dimensional printing in surgery: A systematic review. *Surgery* **2016**, *159*, 1485–1500. [[CrossRef](#)] [[PubMed](#)]
3. Dutta, A.; Singh, M.; Kumar, K.; Navarro, A.R.; Santiago, R.; Kaul, R.P.; Patil, S.; Kalaskar, D.M. Accuracy of 3D printed spine models for pre-surgical planning of complex adolescent idiopathic scoliosis (AIS) in spinal surgeries: A case series. *Ann. 3D Print Med.* **2023**, *11*, 100117. [[CrossRef](#)] [[PubMed](#)]
4. Kuznia, A.L.; Hernandez, A.K.; Lee, L.U. Adolescent Idiopathic Scoliosis: Common Questions and Answers. *Am. Fam. Physician* **2020**, *101*, 19–23. [[PubMed](#)]
5. Arlet, V.; Odent, T.; Aebi, M. Congenital scoliosis. *Eur. Spine J.* **2003**, *12*, 456–463. [[CrossRef](#)]
6. Dias, R.D.; Conboy, H.M.; Gabany, J.M.; Clarke, L.A.; Osterwei, L.J.; Avrunin, G.S.; Arney, D.; Goldman, J.M.; Riccardi, G.; Yule, S.J.; et al. Development of an Interactive Dashboard to Analyze Cognitive Workload of Surgical Teams During Complex Procedural Care. *IEEE Int. Interdiscip. Conf. Cogn. Methods Situat. Aware. Decis. Support.* **2018**, *2018*, 77–82. [[CrossRef](#)]
7. Hussain, A.K.; Kakakhel, M.M.; Ashraf, M.F.; Shahab, M.; Ahmad, F.; Luqman, F.; Ahmad, M.; Nour, A.M.; Varrassi, G.; Kinger, S. Innovative Approaches to Safe Surgery: A Narrative Synthesis of Best Practices. *Cureus* **2023**, *15*, e49723. [[CrossRef](#)]
8. Li, P.; Yang, Z.; Jiang, S. Needle-tissue interactive mechanism and steering control in image-guided robot-assisted minimally invasive surgery: A review. *Med. Biol. Eng. Comput.* **2018**, *56*, 931–949. [[CrossRef](#)]
9. Perfetti, D.C.; Kisinde, S.; Rogers-LaVanne, M.P.; Satin, A.M.; Lieberman, I.H. Robotic Spine Surgery: Past, Present, and Future. *Spine* **2022**, *47*, 909–921. [[CrossRef](#)]
10. Lieberman, I.H.; Kisinde, S.; Hesselbacher, S. Robotic-Assisted Pedicle Screw Placement During Spine Surgery. *JBJS Essent. Surg. Tech.* **2020**, *10*, e0020. [[CrossRef](#)]
11. Mobbs, R.J.; Coughlan, M.; Thompson, R.; Sutterlin, C.E., III; Phan, K. The utility of 3D printing for surgical planning and patient-specific implant design for complex spinal pathologies: Case report. *J. Neurosurg. Spine* **2017**, *26*, 513–518. [[CrossRef](#)] [[PubMed](#)]
12. Izatt, M.T.; Thorpe, P.L.P.J.; Thompson, R.G.; D'urso, P.S.; Adam, C.J.; Earwaker, J.W.S.; Labrom, R.D.; Askin, G.N. The use of physical biomodelling in complex spinal surgery. *Eur. Spine J.* **2007**, *16*, 1507–1518. [[CrossRef](#)] [[PubMed](#)]
13. D'urso, P.S.; Askin, G.; Earwaker, J.S.; Merry, G.S.; Thompson, R.G.; Barker, T.M.; Effeney, D.J. Spinal biomodeling. *Spine* **1999**, *24*, 1247–1251. [[CrossRef](#)] [[PubMed](#)]
14. Parr, W.C.H.; Burnard, J.L.; Wilson, P.J.; Mobbs, R.J. 3D printed anatomical (bio)models in spine surgery: Clinical benefits and value to health care providers. *J. Spine Surg.* **2019**, *5*, 549–560. [[CrossRef](#)] [[PubMed](#)]
15. Kabra, A.; Mehta, N.; Garg, B. 3D printing in spine care: A review of current applications. *J. Clin. Orthop. Trauma.* **2022**, *35*, 102044. [[CrossRef](#)] [[PubMed](#)]
16. Senkoylu, A.; Daldal, I.; Cetinkaya, M. 3D printing and spine surgery. *J. Orthop. Surg.* **2020**, *28*, 2309499020927081. [[CrossRef](#)] [[PubMed](#)]
17. Lenke, L.G.; Betz, R.R.; Harms, J.; Bridwell, K.H.; Clements, D.H.; Lowe, T.G.; Blanke, K. Adolescent idiopathic scoliosis: A new classification to determine extent of spinal arthrodesis. *J. Bone Jt. Surg. Am.* **2001**, *83*, 1169–1181. [[CrossRef](#)]
18. Waran, V.; Narayanan, V.; Karuppiyah, R.; Owen, S.L.; Aziz, T. Utility of multimaterial 3D printers in creating models with pathological entities to enhance the training experience of neurosurgeons. *J. Neurosurg.* **2014**, *120*, 489–492. [[CrossRef](#)] [[PubMed](#)]
19. Galvez, M.; Asahi, T.; Baar, A.; Carcuro, G.; Cuchacovich, N.; Fuentes, J.A.; Mardones, R.; Montoya, C.E.; Negrin, R.; Otayza, F.; et al. Use of Three-dimensional Printing in Orthopaedic Surgical Planning. *J. Am. Acad. Orthop. Surg. Glob. Res. Rev.* **2018**, *2*, e071. [[CrossRef](#)]
20. Jones, T.L.; Hisey, M.S. L5 radiculopathy caused by L5 nerve root entrapment by an L5-S1 anterior osteophyte. *Int. J. Spine Surg.* **2012**, *6*, 174–177. [[CrossRef](#)]
21. Ravi, P.; Burch, M.B.; Farahani, S.; Chepelev, L.L.; Yang, D.; Ali, A.; Joyce, J.R.; Lawera, N.; Stringer, J.; Morris, J.M.; et al. Utility and Costs During the Initial Year of 3D Printing in an Academic Hospital. *J. Am. Coll. Radiol. JACR* **2023**, *20*, 193–204. [[CrossRef](#)] [[PubMed](#)]
22. Wilcox, B.; Mobbs, R.J.; Wu, A.M.; Phan, K. Systematic review of 3D printing in spinal surgery: The current state of play. *J. Spine Surg.* **2017**, *3*, 433–443. [[CrossRef](#)] [[PubMed](#)] [[PubMed Central](#)]
23. Smith, T.; Evans, J.; Moriel, K.; Tihista, M.; Bacak, C.; Dunn, J.; Rajani, R.; Childs, B. The Cost of OR Time is \$46.04 per Minute. *J. Orthop. Bus.* **2022**, *2*, 10–13. [[CrossRef](#)]
24. Childers, C.P.; Maggard-Gibbons, M. Understanding Costs of Care in the Operating Room. *JAMA Surg.* **2018**, *153*, e176233. [[CrossRef](#)] [[PubMed](#)]
25. Waqar, A.; Othman, I.; Almujiabah, H.R.; Sajjad, M.; Deifalla, A.; Shafiq, N.; Azab, M.; Qureshi, A.H. Overcoming implementation barriers in 3D printing for gaining positive influence considering PEST environment. *Ain Shams Eng. J.* **2024**, *15*, 102517. [[CrossRef](#)]

26. Hellman, S.; Frisch, P.; Platzman, A.; Booth, P. 3D Printing in a hospital: Centralized clinical implementation and applications for comprehensive care. *Digit. Health* **2023**, *9*, 20552076231221899. [[CrossRef](#)] [[PubMed](#)] [[PubMed Central](#)]
27. Davies, S. Standard of care: Why hospital-based 3D printing labs are becoming so prevalent. In *TCT Magazine: 3D Printing & Additive Manufacturing Intelligence*; Rapid News Publications Ltd.: Chester, UK, 2021. Available online: <https://www.tctmagazine.com/additive-manufacturing-3d-printing-industry-insights/healthcare-medical-dental-and-bioprinting-insights/standard-of-care-hospital-3d-printing-labs-prevalent/> (accessed on 27 February 2024).

Disclaimer/Publisher's Note: The statements, opinions and data contained in all publications are solely those of the individual author(s) and contributor(s) and not of MDPI and/or the editor(s). MDPI and/or the editor(s) disclaim responsibility for any injury to people or property resulting from any ideas, methods, instructions or products referred to in the content.